

# Deformation of Trapped Fermi Gases with Unequal Spin Populations

Guthrie B. Partridge<sup>1</sup>, Wenhui Li<sup>1</sup>, Yean-An Liao<sup>1</sup>, Randall G. Hulet<sup>1</sup>, Masudul Haque<sup>2</sup> & H. T. C. Stoof<sup>2</sup>

<sup>1</sup>*Department of Physics and Astronomy and Rice Quantum Institute, Rice University, Houston, TX 77251, USA.*

<sup>2</sup>*Institute for Theoretical Physics, Utrecht University, Leuvenlaan 4, 3584 CE Utrecht, the Netherlands.*

The formation of electron pairs, each pair consisting of a spin-up and a spin-down electron, underlies the phenomenon of superconductivity. While the population of each spin component is generally equal in superconductors, an imbalance is readily produced in experiments with gases of trapped, ultracold fermionic atoms, as was recently demonstrated<sup>1,2</sup>. Exotic new states of matter are predicted for the unbalanced system that, if realized, may have important implications for our understanding of nuclei, compact stars, and quantum chromodynamics. We previously reported evidence for a phase separation in a strongly-interacting two-component Fermi gas to a state containing a paired central core, with the excess unpaired atoms residing outside this core<sup>2</sup>. We show here that the real-space distributions of the gas deform markedly with increasing imbalance in order to produce a core that is uniformly paired. These deformations are inconsistent with local space isotropy as embodied by the local-density approximation (LDA). The breakdown of the LDA is surprising as the correlation length is small compared with the characteristic size of the gas. A possible explanation, considered here, is that an

**anisotropic nematic ordering develops. The observed violations of the LDA may be facilitated by the high aspect ratio trapping geometry employed in the experiment. We find that these deformations can be suppressed at higher temperature.**

Phase separation, such as the separation of the liquid and vapour phases of water, is a common occurrence. Calculations show that a trapped, two-component Fermi gas with unequal numbers may also phase separate<sup>3-7</sup>, and as we previously reported, such a phase separation can be detected experimentally in the real-space atomic distributions obtained by *in-situ* (in the trap) imaging<sup>2</sup>. In particular, a uniformly paired region produces a minimum in the difference distribution, obtained by subtracting the majority and minority spin densities. Shin *et al.* have recently adopted *in-situ* imaging, and present their resulting images as evidence for phase separation<sup>8</sup>. In our previous work, we found that the appearance of a central minimum in the difference images was accompanied by a corresponding central dip in the axial density profile obtained by integrating the two-dimensional column density along the radial coordinate<sup>2</sup>. It was pointed out, however, that under the assumptions of LDA and harmonic confinement, a uniformly paired core would produce a constant axial density difference, rather than a central dip<sup>9,10</sup>. Several authors have calculated spatial distributions for phase separation, assuming both a harmonic trapping potential and the LDA<sup>11-15</sup>. In the experiment, axial confinement, formed mainly by magnetic curvature and to a lesser extent by a focused infrared laser beam, was harmonic to good approximation. Radial confinement, on the other hand, was produced by the Gaussian waist of the laser beam, resulting in an effectively anharmonic potential. Radial anharmonicity causes spreading in the radial direction, primarily for the majority spin component, and hence produces a *peaking* of the difference axial density profile, and not a dip. We noted in ref. 2 that the excess unpaired atoms reside primarily at the axial poles of the highly-elongated trap, while relatively few occupy the equatorial shell, in

violation of the LDA. In this paper, we present detailed quantitative measurements of the deformation as a function of number mismatch, and by reconstruction of the three-dimensional (3D) density distributions, explore the properties of the phase-separated state.

Our apparatus and methods for producing a strongly-interacting, two-component Fermi gas of  ${}^6\text{Li}$  atoms has been described previously<sup>2,16</sup>. The relative population of two hyperfine states, designated as  $|1\rangle$  and  $|2\rangle$ , is controlled by driving radio-frequency transitions between them. Spin relaxation is negligible over the duration of the experiment. A nearly uniform magnetic field is tuned to the location of a broad Feshbach resonance at 834 G<sup>17,18</sup>, where the two-body scattering length diverges ( $\pm\infty$ ) producing unitarity-limited strong interactions. The combined optical and magnetic potential is given by

$$U(r, z) = \frac{1}{2} m \omega_B^2 z^2 + U_o \left( 1 - \frac{w_o^2}{w^2(z)} e^{-\frac{2r^2}{w^2(z)}} \right), \quad (1)$$

where  $\omega_B = (2\pi) 6.5$  Hz,  $w_o = 26$   $\mu\text{m}$ ,  $w(z) = w_o [1 - (z/z_o)^2]^{1/2}$ , and  $z_o = 1.7$  mm. Both radial and axial potentials are approximately harmonic for sufficiently small  $r$  and  $z$ . By reducing the laser intensity until  $U_o$  achieves its final value of 544 nK, the atoms are evaporatively cooled. At this trap depth, the radial and axial trap frequencies are  $\omega_r = (2\pi) 325$  Hz and  $\omega_z = (2\pi) 7.2$  Hz, respectively. The two states,  $|1\rangle$  and  $|2\rangle$ , are sequentially imaged in the trap by absorption. The first optical probe pulse breaks pairs, and thereby causes a small heating that radially broadens the second images. We have reduced the delay between probe pulses to 27  $\mu\text{s}$ , significantly reducing the effect of probe-induced heating previously observed for delays of 215  $\mu\text{s}$ <sup>2</sup>. Analysis of the images provides measurement of the number of atoms in each state,  $N_1$  and  $N_2$ , from which the polarization  $P = (N_1 - N_2) / (N_1 + N_2)$  may be determined. By fitting the resulting profiles to fermionic nonzero-temperature

Thomas-Fermi distributions, we obtain effective temperatures of  $\tilde{T} < 0.05 T_F$ , where  $T_F$  is the Fermi temperature. The actual temperatures are expected to be closely related to  $\tilde{T}$ <sup>19</sup>.

Figure 1 shows a series of images corresponding to a range of  $P$  from 0 to 0.95. The minority spin ( $|2\rangle$ ) distribution becomes markedly less elongated with increasing  $P$ , while its radial size remains approximately the same as that for the majority spin ( $|1\rangle$ ). This deformation causes the bunching of unpaired atoms at the axial poles, and a lack of them in the equatorial shell, as observed previously<sup>2</sup>. Remarkably, the deformation grows up to the highest observed polarization. The central holes in the difference distributions, which are approximately equal to the background level for all but the highest values of  $P$ , indicate that the central core is nearly uniformly paired. Figure 2 shows the aspect ratio for both states. While the majority state aspect ratio changes little, that of the minority (representing the core) decreases by a factor of 10 when going from completely unpolarized ( $P = 0$ ) to completely polarized ( $P = 1$ ).

Figure 3a presents a centre-line cut of the column densities of the majority and minority states, as well as their difference, taken along the axial direction. The axial density difference profile of this data also exhibits a pronounced central dip, as in ref. 2. A sharp phase boundary between the core and excess fermions is readily apparent in Fig. 3a, indicating that a partially polarized shell, if it exists, is extremely thin. This observation of a sharp phase boundary contrasts with the observations reported in ref. 8. Unlike the core region, the wings of the unpaired atom distribution fit well to a fermionic Thomas-Fermi distribution. Cylindrical symmetry of the trap enables reconstruction of the true 3D density distribution  $n(r, z)$  from the column densities by use of the inverse Abel transform<sup>20</sup>. An axial cut of the reconstructed 3D density,  $n(r = 0, z)$ , is shown in Figure 3b. The ratio of the central densities,  $n_1(0,0)/n_2(0,0)$ , may be obtained from the reconstructed 3D

distributions, and are plotted vs.  $P$  in Figure 4a. The central core remains unpolarized until at least  $P \approx 0.9$ , in contradiction to the results reported in ref. 8, where uniform pairing was observed to breakdown at  $P \approx 0.77$ .

The observed LDA-violating deformations are surprising, because the radial size of the distributions is about 10 times larger than the inverse Fermi momentum  $k_F^{-1}$ , the expected magnitude of the correlation length. Nonetheless, there are several LDA-violating mechanisms, enhanced by confinement in a high aspect ratio trapping potential, that may explain these observations. De Silva and Mueller have shown that surface tension between the normal and superfluid phases can result in deformations of the minority component that are quite similar to those observed here<sup>21</sup>. Also, gradient terms in the Gross-Pitaevskii equation can lead to LDA-violating deformations on the BEC side of resonance, although the magnitude of the calculated effect is much smaller than we observe at unitarity<sup>22</sup>. Finally, we have explored whether a deformed Fermi surface (DFS)<sup>23</sup>, can explain the data. With a DFS, the rotational symmetry of the local Fermi surfaces is broken causing the appearance of anisotropic or nematic ordering. If this nematic order depends on position, it can lead to a macroscopic deformation of both the minority and the majority density profiles. We use a WKB approximation to determine the deformed local chemical potentials for a given elliptical shape of the two clouds. These are used to calculate the superfluid order parameter and the local spin densities, within mean-field theory. For  $P \neq 0$  and at zero temperature, we find that the gas always phase separates and consists of a DFS superfluid core with normal regions at the axial poles. The optimal shape of the two clouds is found by minimizing the total thermodynamic potential of the gas, including a phenomenological surface energy of the superfluid-normal interface. The circles in Figure 3a are the results of this calculation, which compare quite favourably with experiment.

We had previously found that phase separation occurred only for  $P > P_c$ , where  $P_c \approx 0.1^2$ . For  $P < P_c$ , the observations were consistent with a non-phase-separated polarized superfluid. The present data, however, exhibits phase separation for arbitrarily small  $P$ . Since the previous work, we have improved the efficiency of the evaporation trajectory, and now obtain fitted temperatures that are about half of those previously attained. This temperature-dependent behaviour is consistent with a phase boundary between a phase-separated regime and a polarized superfluid (Sarma or breached-pair phase)<sup>24-26</sup> at nonzero temperature. Such a phase boundary has recently been discussed in the context of a tricritical point in the phase diagram<sup>13,27-29</sup>. To test this hypothesis, we deliberately produced higher temperatures by stopping the evaporation trajectory at a higher trap depth (1.2  $\mu$ K), resulting in  $\tilde{T} \approx 0.25 T_F$ . Figure 4b shows that the central densities in this case remain equal until a critical polarization of  $P \approx 0.7$  is reached. This higher temperature result is consistent with that reported in ref. 8.

Figure 5 shows absorption images prepared at both the lower and higher temperatures. It is readily apparent from the images that the density distributions of the two components of the higher temperature gas show no deformations, in contrast to those of the colder case. We find that at higher temperatures, the aspect ratios of the minority and majority components remain equal and constant for all  $P$ . This lack of deformation is also evident in the axial density distributions, where in the case of the colder data, the axial difference distribution (Figure 5b) shows the characteristic double peaked structure observed previously<sup>2</sup>, while that of the warmer cloud (Figure 5d) exhibits the flat-topped distribution predicted under the assumption of LDA<sup>9,10</sup>. The phase boundary is also much sharper for the low temperature data. In summary, the higher temperature data are consistent with the results presented in ref. 8, and support the suggestion of a temperature

dependent transition between a low-temperature phase separated state and a higher temperature polarized superfluid<sup>29</sup>.

We have reported that pairing with unequal spin populations leads to real-space deformations in a highly elongated, but still three-dimensional geometry. The sharp phase boundaries between the superfluid core and the polarized normal phase are consistent with the usual convention that phase separation is associated with first-order phase transitions, while for a second-order transition, mixing is possible and we would not expect sharp boundaries between the phases. In a higher temperature polarized gas, these deformations are absent, though a uniformly paired core remains.

**Acknowledgements.** We thank E. Mueller for helpful discussions and for providing the Abel transform code. Support was provided by the U.S. National Science Foundation, the National Aeronautics and Space Administration, the Office of Naval Research, the Welch Foundation, the Stichting voor Fundamenteel Onderzoek der Materie (FOM), and the Nederlandse Organisatie voor Wetenschappelijk Onderzoek (NWO).

**Author's contributions.** G.B.P. and W.L. contributed equally to this work.

Correspondence and requests for materials should be addressed to R.G.H. (e-mail: randy@rice.edu).

**Figure 1** *In-situ* absorption images for a polarized Fermi gas. The top figure of each sequence corresponds to the column density of state  $|1\rangle$ , the middle to state  $|2\rangle$ , and the third to the difference of the two. The polarizations are **a**,  $P = 0$ , **b**,  $P = 0.18$ , **c**,  $P = 0.37$ , **d**,  $P = 0.60$ , **e**,  $P = 0.79$ , and **f**,  $P = 0.95$ . In each sequence, state  $|2\rangle$  was imaged first, followed by state  $|1\rangle$ . Slight probe-induced heating can be discerned in the images of state  $|1\rangle$ , where the distribution bulges slightly in the radial direction in the region of overlap between the two states. The field of view for these images is 1654  $\mu\text{m}$  by 81  $\mu\text{m}$ . The displayed aspect ratio was reduced by a factor of 4.4 for clarity. Note that the apparent inversion of aspect ratio of the minority state in **e** is a result of this scaling.

**Figure 2** Aspect ratio vs. polarization. The aspect ratio of the axial to the radial dimensions,  $R_z/R_r$ , is shown for state  $|1\rangle$  by the black circles and for state  $|2\rangle$  by the red crosses. The radii  $R_r$  for both states are determined by fitting the column density profiles to zero-temperature, fermionic Thomas-Fermi distributions. The axial distributions are distinctly non-Thomas-Fermi-like, so  $R_z$  is found by a simple linear extrapolation of the column density to zero. An aspect ratio of 36 is the expected value for a non-interacting gas with anharmonic corrections, in reasonable agreement with the observations. The uncertainty in  $P$  is 0.04, which is the standard deviation of polarization measurements deliberately prepared as  $P = 0$ . There are shot to shot variations in  $N_1$  and a small systematic variation towards larger  $N_1$  at smaller  $P$ . For  $P < 0.40$ ,  $N_1 = 170 \text{ k} \pm 40 \text{ k}$ , and for  $P > 0.40$ ,  $N_1 = 135 \text{ k} \pm 25 \text{ k}$ , where the uncertainty is the standard deviation of the measurements. The corresponding average Fermi temperature is  $T_F \approx 430 \text{ nK}$ , where we define  $T_F = \hbar(\omega_r^2 \omega_z)^{1/3} (6N_1)^{1/3}/k_B$ .

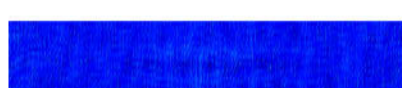
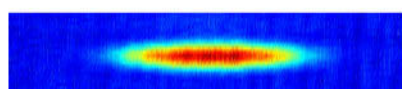
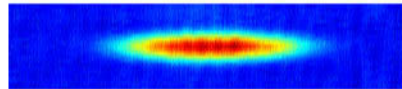
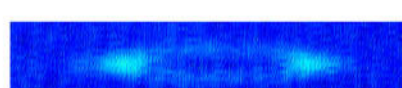
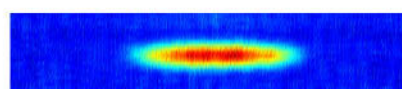
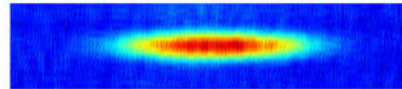
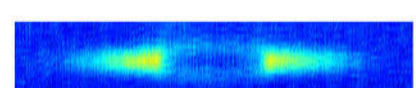
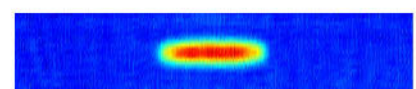
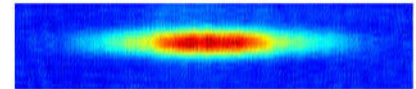
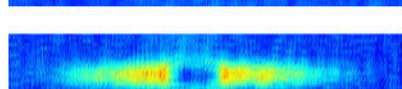
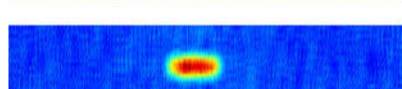
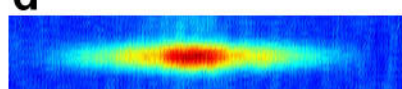
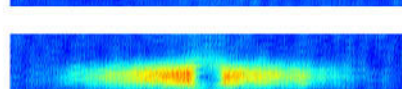
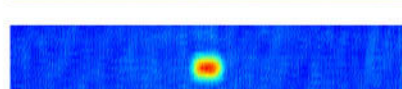
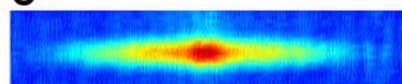
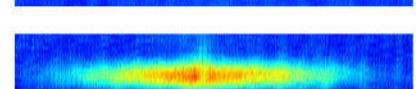
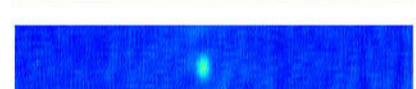
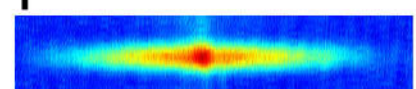
**Figure 3 Column-density profile and 3d density reconstruction.** The black lines correspond to state  $|1\rangle$ , the red to state  $|2\rangle$ , and the green to their difference, for  $P = 0.35$  and  $N_1 = 175$  k. The circles are the results of a calculation assuming a deformed Fermi surface (see text). **a**, Centre-line ( $r = 0$ ) axial cut of the column-densities. **b**, Centre-line axial cut of the reconstructed 3D densities. The signal to noise of **b** was improved by reflecting and averaging the column density images about both the  $r = 0$  and the  $z = 0$  planes before reconstruction.

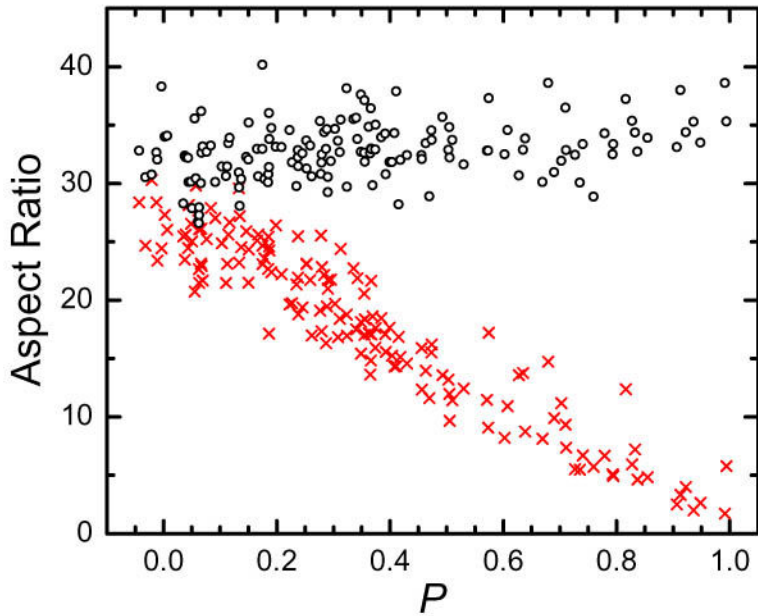
**Figure 4 Ratio of the central densities vs. polarization.** **a**,  $\tilde{T} < 0.05 T_F$ , corresponding to the data shown in Figure 2; **b**,  $\tilde{T} \cong 0.25 T_F$ , with average  $N_1 = 500$  k. The dotted lines correspond to  $[(1+P)/(1-P)]^{1/2}$ , the expected central density ratio for a harmonically confined, non-interacting gas at  $T = 0$ . The solid line indicates equal central densities. The sudden jump in  $n_1(0,0)/n_2(0,0)$  in **a** for  $P > 0.9$  may be explained by higher temperatures for these data that arise from inefficiencies in evaporative cooling at very high  $P$ .

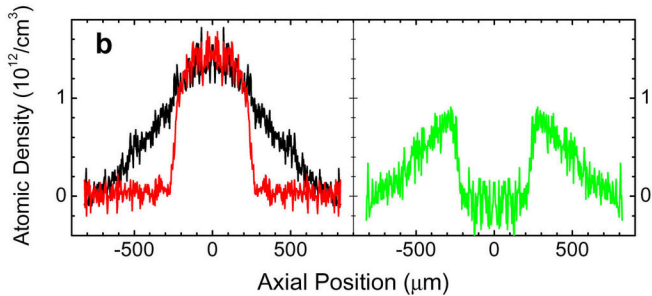
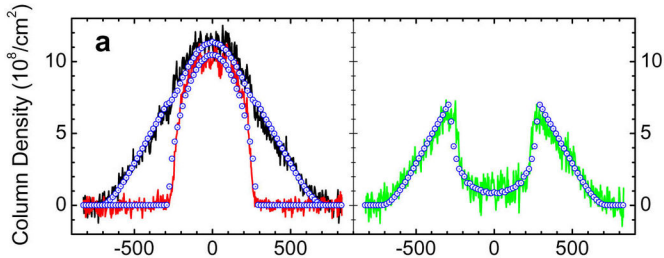
**Figure 5 In-situ absorption images and integrated profiles.** To the left are absorption images, while the plots to the right are the corresponding axial density distributions. **a,b**:  $P = 0.50$ ,  $N_1 = 146$  k, with  $\tilde{T} < 0.05 T_F$ ; **c,d**:  $P = 0.45$ ,  $N_1 = 374$  k, with  $\tilde{T} \cong 0.25 T_F$ .

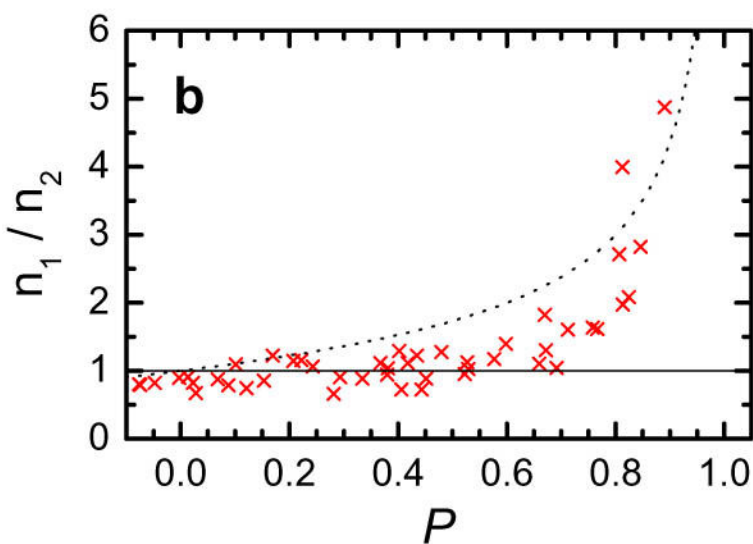
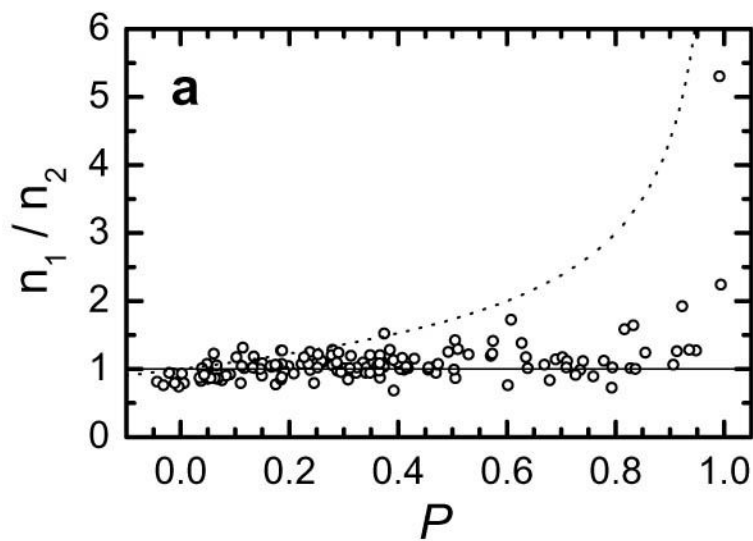
1. Zwierlein, M. W., Schirotzek, A., Schunck, C. H. & Ketterle, W. Fermionic Superfluidity with Imbalanced Spin Populations. *Science* **311**, 491-6 (2006).
2. Partridge, G. B., Li, W., Kamar, R. I., Liao, Y. A. & Hulet, R. G. Pairing and Phase Separation in a Polarized Fermi Gas. *Science* **311**, 503-5 (2006).
3. Bedaque, P. F., Caldas, H. & Rupak, G. Phase Separation in Asymmetrical Fermion Superfluids. *Physical Review Letters* **91**, 247002-1-4 (2003).
4. Carlson, J. & Reddy, S. Asymmetric Two-component Fermion Systems in Strong Coupling. *Physical Review Letters* **95**, 060401-1-4 (2005).
5. Sheehy, D. E. & Radzhovsky, L. BEC-BCS Crossover in "Magnetized" Feshbach-Resonantly Paired Superfluids. *Physical Review Letters* **96**, 060401-1-4 (2006).
6. Gu, Z.-C., Warner, G. & Zhou, F. Fermion pairing with population imbalance: energy landscape and phase separation in a constrained Hilbert subspace. *cond-mat/0603091* (2006).
7. Hu, H. & Liu, X.-J. Mean-field phase diagrams of imbalanced Fermi gases near a Feshbach resonance. *Physical Review A* **73**, 051603-1-4 (2006).
8. Shin, Y., Zwierlein, M. W., Schunck, C. H., Schirotzek, A. & Ketterle, W. Observation of Phase Separation in a Strongly-Interacting Imbalanced Fermi Gas. *Phys. Rev. Lett.* **97**, 030401-1-4 (2006).
9. De Silva, T. N. & Mueller, E. J. Profiles of near-resonant population-imbalanced trapped Fermi gases. *Physical Review A* **73**, 051602-1-4 (2006).
10. Haque, M. & Stoof, H. T. C. Pairing of a trapped resonantly-interacting fermion mixture with unequal spin populations. *Physical Review A* **74**, 011602-1-4 (2006).
11. Pieri, P. & Strinati, G. C. Trapped Fermions with Density Imbalance in the Bose-Einstein Condensate Limit. *Physical Review Letters* **96**, 150404-1-4 (2006).
12. Yi, W. & Duan, L.-M. Trapped fermions across a Feshbach resonance with population imbalance. *Physical Review A* **73**, 031604-1-4 (2006).
13. Chevy, F. Density Profile of a Trapped Strongly Interacting Fermi Gas with Unbalanced Spin Populations. *Physical Review Letters* **96**, 130401-1-4 (2006).
14. Pao, C.-H. & Yip, S.-K. Asymmetric Fermi superfluid in a harmonic trap. *Journal of Physics: Condensed Matter* **18**, 5567-5577 (2006).
15. Chien, C.-C., Chen, Q., He, Y. & Levin, K. Finite temperature effects in trapped Fermi gases with population imbalance. *cond-mat/0605684* (2006).

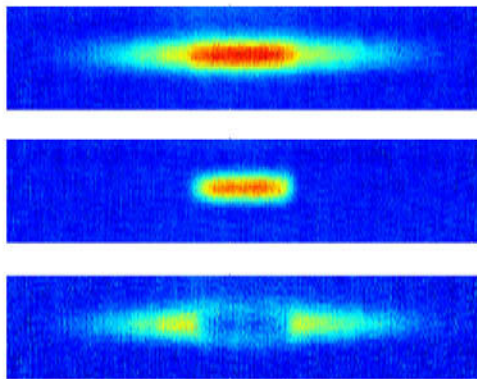
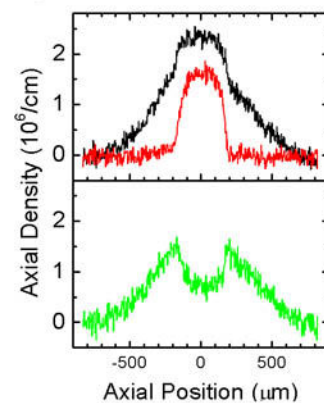
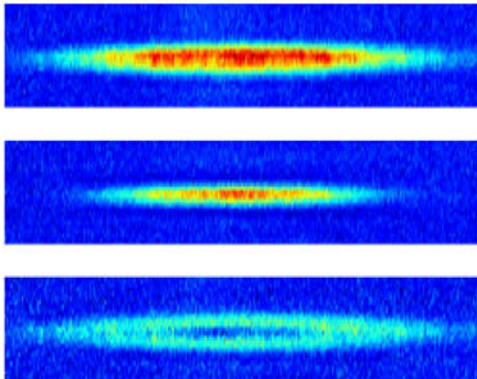
16. Partridge, G. B., Strecker, K. E., Kamar, R. I., Jack, M. W. & Hulet, R. G. Molecular Probe of Pairing in the BEC-BCS Crossover. *Physical Review Letters* **95**, 020404-1-4 (2005).
17. Houbiers, M., Stoof, H. T. C., McAlexander, W. I. & Hulet, R. G. Elastic and inelastic collisions of  $^6\text{Li}$  atoms in magnetic and optical traps. *Physical Review A* **57**, R1497-1500 (1998).
18. Bartenstein, M. et al. Precise Determination of  $^6\text{Li}$  Cold Collision Parameters by Radio-Frequency Spectroscopy of Weakly Bound Molecules. *Physical Review Letters* **94**, 103201-1-4 (2005).
19. Kinast, J. et al. Heat Capacity of a Strongly Interacting Fermi Gas. *Science* **307**, 1296-1299 (2005).
20. Smith, L. M., R., K. D. & Sudharsanan, S. I. Abel Inversion Using Transform Techniques. *Journal of Quantitative Spectroscopy and Radiative Transfer* **39**, 367-373 (1988).
21. De Silva, T. N. & Mueller, E. J. Surface tension in population imbalanced unitary Fermi gases. *Physical Review Letters* **97**, 070402-1-4 (2006).
22. Imambekov, A., Bolech, C. J., Lukin, M. & Demler, E. Breakdown of the Local Density Approximation in Interacting Systems of Cold Fermions in Strongly Anisotropic Traps. *cond-mat/0604423* (2006).
23. Sedrakian, A., Mur-Petit, J., Polls, A. & Müther, H. Pairing in a two-component ultracold Fermi gas: Phases with broken-space symmetries. *Physical Review A* **72**, 013613-1-8 (2005).
24. Sarma, G. On the Influence of a Uniform Exchange Field Acting on the Spins of the Conduction Electrons in a Superconductor. *Journal of Physics and Chemistry of Solids* **24**, 1029-1032 (1963).
25. Houbiers, M. et al. The Superfluid State of Atomic  $^6\text{Li}$  in a Magnetic Trap. *Physical Review A* **56**, 4864-4878 (1997).
26. Liu, W. V. & Wilczek, F. Interior Gap Superfluidity. *Physical Review Letters* **90**, 047002-1-4 (2003).
27. Combescot, R. & Mora, C. The low-temperature Fulde-Ferrell-Larkin-Ovchinnikov phases in 3 dimensions. *Europhysics Letters* **68**, 79-85 (2004).
28. Parish, M. M., Marchetti, F. M., Lamacraft, A. & Simons, B. D. Finite temperature phase diagram of a polarised Fermi condensate. *cond-mat/0605744* (2006).
29. Gubbels, K. B., Romans, M. W. J. & Stoof, H. T. C. Sarma Phase in Trapped Unbalanced Fermi Gases. *cond-mat/0606330* (2006).

**a****b****c****d****e****f**







**a****b****c****d**